



ORIGINAL ARTICLE

Sustainable fabrication of silver-titania nanocomposites using goji berry (*Lycium barbarum* L.) fruit extract and their photocatalytic and antibacterial applications



Abdulrahman Ahmed Sharwani^a, Kannan Badri Narayanan^{a,c,*},
Mohammad Ehtisham Khan^b, Sung Soo Han^{a,c,*}

^a School of Chemical Engineering, Yeungnam University, 280 Daehak-Ro, Gyeongsan, Gyeongbuk 38541, Republic of Korea

^b Department of Chemical Engineering Technology, College of Applied Industrial Technology (CAIT), Jazan University, Jazan 45971, Saudi Arabia

^c Research Institute of Cell Culture, Yeungnam University, 280 Daehak-Ro, Gyeongsan, Gyeongbuk 38541, Republic of Korea

Received 26 July 2021; accepted 21 September 2021

Available online 29 September 2021

KEYWORDS

Nanocomposites;
Silver;
Titania;
Goji berries;
Antibacterial;
Photocatalyst

Abstract Silver-titania nanocomposites (Ag-TiO₂ NCs) have unique functional attributes due to their photocatalytic and antibacterial properties. In this study, titania nanoparticles (TiO₂-NPs) were successfully *in-situ* decorated with silver nanoparticles (Ag-NPs) using the aqueous extract of goji berries (*Lycium barbarum* L.) as a bioreducing and stabilizing agent. Different Ag-TiO₂ NCs were synthesized by treating different concentrations of silver nitrate with a specific concentration of TiO₂-NPs in the presence of fruit extract. The green-synthesized NCs were characterized using several techniques viz., ultraviolet–visible spectrophotometry, X-ray diffractometry (XRD), scanning electron microscopy, field-emission transmission electron microscopy (FE-TEM), Fourier transform infrared spectroscopy, and X-ray photoelectron spectroscopy. XRD analysis revealed the formation of face-centered cubic (fcc) crystals, and FE-TEM analysis revealed the embedment of Ag-NPs throughout the surface of TiO₂-NPs. The average size of Ag-NPs on TiO₂-NPs increased from 11.2 ± 3.05 nm to 16.4 ± 4.5 nm with an increase in the concentration of silver ions, and the morphology of Ag-NPs was predominantly quasi-spherical and hexagonal. These NCs exhibited an excellent photocatalytic degradation of an azo dye, methylene blue (MB). The synthesized Ag-TiO₂ NCs (3:1) showed higher photocatalytic degradation efficiency of ~ 93.4% for MB in 130 min under visible light irradiation. Ag-TiO₂ NCs also exhibited good antibacterial activities towards

* Corresponding authors.

E-mail addresses: okbadri@gmail.com (K. Badri Narayanan), sshan@yu.ac.kr (S. Soo Han).

Peer review under responsibility of King Saud University.



Staphylococcus aureus (Gram-positive) and *Escherichia coli* (Gram-negative). Therefore, the formation of Ag-NPs on the surface of TiO₂-NPs to form Ag-TiO₂ NCs exhibits eco-friendly photocatalytic degradation of azo dye contaminants as well as antibacterial activity.

© 2021 The Author(s). Published by Elsevier B.V. on behalf of King Saud University. This is an open access article under the CC BY-NC-ND license (<http://creativecommons.org/licenses/by-nc-nd/4.0/>).

1. Introduction

The fundamental research in the development of unique and promising nanocomposite materials has gained much attention in recent years and twined with interdisciplinary fields of chemistry, physics, biology, and material science. Nanocomposites (NCs) are an amalgamation of different materials to develop unique properties of the materials ensuring the size of one of the materials below 100 nm. Thus, these NCs have markedly different electrochemical, magnetic, catalytic, optical, and biological properties from the component materials (Camargo et al., 2009). Solution-based, vapor-phase and gas-phase syntheses are the commonly used synthetic methods, which are further divided based on top-down and bottom-up approaches. Moreover, they are synthesized based on physical, chemical, biological, and hybrid methods (Gudikandula and Charya Maringanti, 2016; Mohammad et al., 2019). Although physical and chemical methods are commonly used, the use of expensive processes and toxic and harmful chemicals greatly restricts their applications, particularly in environmental and biomedical applications (Natsuki et al., 2015).

Titanium (TiO₂) is a wide-bandgap semiconducting metal oxide in different crystalline structures namely rutile, anatase, and brookite. TiO₂ is widely used in different types of nanomaterials because of its photocatalytic abilities and its interaction with biological molecules (Bakbolat et al., 2020). Different bottom-up approaches viz., co-precipitation, sol-gel, and hydrothermal methods are commonly used as cost-effective methods for the synthesis of metal oxide NCs. The incorporation of different noble metals, such as silver (Ag), gold (Au), platinum (Pt), and palladium (Pd) as dopants in the synthesis of TiO₂ NCs increases the photocatalytic reactivity (Cozzoli et al., 2004), in particular, Ag and Au are the most commonly used noble metals in combination with TiO₂ NCs. The use of Ag-TiO₂ NC films showed 6.3-fold increased photocatalytic degradation of methyl orange compared to bare TiO₂ films under ultraviolet (UV) illumination (Yu et al., 2005). Similarly, Au-TiO₂ NCs microspheres showed improved photocatalytic degradation of antibiotic pollutant, ciprofloxacin under UV, and visible illuminations (Martins et al., 2020). Along with photocatalytic behavior, TiO₂ nanoparticles (NPs) have documented bactericidal activity by the generation of reactive oxygen species (ROS) that oxidize bacterial membrane lipids by lipid peroxidation under UV illumination (Kikuchi et al., 1997). Thus, Ag-TiO₂ NCs exhibited enhanced photocatalytic and bactericidal activities compared to the bare TiO₂ nanoparticles (NPs) (Zhang and Chen, 2009).

Embracing green and sustainable methodology in the synthesis of metal oxide NCs is an emerging and pressing priority research avenue relevant for green chemistry principles (Dhingra et al., 2010). The main advantages of green methods are their cost-effectiveness, non-toxic, and eco-friendly compared to physical and chemical methods. The extracts of plant

entities are the prime source for the green synthesis of a myriad of nanomaterials. The constituents of these extracts contain several metabolites, viz., polyphenols, terpenoids, sugars, alkaloids, phenolic acids, and proteins, which can directly involve in the bioreduction and stabilization processes (Ahmed et al., 2016a; Aswathy Aromal and Philip, 2012). Zahir et al., (2015) demonstrated the green synthesis of Ag- and TiO₂-NPs, using *Euphorbia prostrata* plant extract, as antileishmanial agents. Recently, Ag-TiO₂ NC was synthesized using the leaf extract of *Origanum majorana* under ultrasound irradiation (Bhardwaj and Singh, 2021). There are several reports even for the synthesis of Ag-NPs using plant/fruit extracts of *Citrullus lanatus* (watermelon) (Ndikau et al., 2017), *Avena sativa* (oat) (Amini et al., 2017), *Prangos ferulaceae* (Habibi et al., 2017), *Gmelina arborea* (Kashmir tree) (Saha et al., 2017), *Parkia speciosa* (bitter bean) (Fatimah, 2016), and *Azadirachta indica* (neem) (Ahmed et al., 2016b) with antibacterial and antioxidant activity. Hence, we put forth our efforts to explore the green synthesis of metal oxide NCs. Greener synthesis of Ag-TiO₂ nanocomposite was reported using the extracts of *Carpobrotus acinaciformis* (leaf and flower) (Rostami-Vartooni et al., 2016), *Euphorbia heterophylla* (leaf) (Atarod et al., 2016), *Uncaria gambir* Roxb (leaf) (Wahyuni et al., 2019), and by electrochemically active biofilm (Khan et al., 2013). These NCs were also involved in the degradation of various organic pollutants, such as 4-nitrophenol, methylene blue, methyl orange, congo red, and rhodamine B. The superfood “goji berries” are prevalent widely in arid to semi-arid countries, and the extract of goji berries has potential antioxidant and antimicrobial properties along with anticancer and immunomodulatory effects (Ilic et al., 2020). Previously, Dong et al., (2017) demonstrated the green synthesis of Ag-NPs using the extract of wolfberry fruit extract. In this study, we have used the aqueous fruit extract of red goji berries (*Lycium barbarum* L.) as a natural bioreducing and stabilizing agent for the first time, for the fabrication of noble metal-decorated metal oxide NCs i.e., silver-titanium NCs (Ag-TiO₂ NCs) and evaluated their photocatalytic degradation of an azo dye (methylene blue) as well as the antibacterial potential against *Staphylococcus aureus* and *Escherichia coli*.

2. Experimental

2.1. Materials

Silver nitrate (AgNO₃, 99%), bare titanium nanoparticles (TiO₂-NPs, size ~ 21 nm), sodium hydroxide (NaOH), ampicillin, and methylene blue (MB) were purchased from Sigma-Aldrich (USA). Dried red goji berries (*Lycium barbarum* L.) were obtained from Yeongcheon medicinal herb market (Yeongcheon, South Korea). Mueller-Hinton (MH) broth and agar were purchased from Becton, Dickinson, and Company (MD, USA). The bacterial strains of *Escherichia coli*

(KCTC 2571) and *Staphylococcus aureus* (KCTC 3881) from the Korean Collection for Type Cultures (KCTC) (Jeollabuk, South Korea) were used in this study. All the solutions were prepared using the deionized (DI) water obtained from the Milli-Q water purification system (Merck Millipore).

2.2. Preparation of goji berries (*Lycium barbarum* L.) extract

Initially, the glassware for the experiment was washed and rinsed with deionized water and then dried to avoid any kind of contamination. The dried red goji berries (GB) were cut into small parts and excellently ground with mortar and pestle. The 5.0 g of powdered GB were put into an Erlenmeyer flask (250 mL) containing 100 mL of deionized water and boiled with stirring for 15 min. Later, the resultant solution was centrifuged at a speed of 4,000 rpm for 10 min, and the supernatant of the fruit extract was filtered three times using gravity through Whatman qualitative filter paper (Grade 1) to obtain a clarified GB solution. Thus, the obtained aqueous fruit extract was kept at 4 °C for the fabrication of silver-titania nanocomposites (Ag-TiO₂ NCs).

2.3. Sustainable fabrication of silver-titania nanocomposites (Ag-TiO₂ NCs)

Three millimolar of bare TiO₂-NPs were dispersed in 90 mL of deionized water and sonicated for 30 min. To this, different concentrations of AgNO₃ (0.5, 1.0, and 1.5 mM) were added as a metal precursor and sonicated again for 10 min. Then, 10 mL of freshly prepared GB extract was added, and the pH of the solution was adjusted to 7.0 with 0.1 N NaOH solution. The resultant mixture was subjected to vigorously stirring for 24 h at room temperature. After 24 h of reaction, the solution was centrifuged at 10,000 rpm for 20 min (Model: 1580R, LaboGene, Daejeon, South Korea), and the pellet was washed with absolute ethanol. Finally, the synthesized Ag-TiO₂ NCs (3:0.5, 3:1, and 3:1.5) were dried in a vacuum oven (JS Research Inc., Chungchungnam-do, South Korea) at 60 °C for 20 h and stored in a sterile airtight vial.

2.4. Characterization of Ag-TiO₂ NCs

The absorption spectra of TiO₂-NPs and different Ag-TiO₂ NCs were obtained using a double beam ultraviolet–visible–near infrared (UV–vis–NIR) spectrophotometer (VARIAN, Cary 5000, USA) over the range of 200–800 nm. The powder X-ray diffraction (XRD) was measured to check the crystallinity of Ag-TiO₂ NCs using a PANalytical X'Pert PRO MPD using CuK α 1 radiation with a wavelength of 1.5406 Å at the tube voltage of 40 kV and the tube current of 30 mA in the scan range of 20.0°–80.0° at the scan rate of 1.2° per min. All the diffraction peaks of the crystalline phases were compared with those of standard compounds reported in the JCPDS data file. The average crystallite size was calculated using the Debye–Scherrer's formula: $D = 0.9 \lambda / \beta \cos \theta$, λ , X-ray wavelength; β , the line broadening at half the maximum intensity (FWHM) and θ is the Bragg's angle. For Fourier transform infrared (FT-IR) spectra, the transmittance measurements of dried samples of Ag-TiO₂ NCs between the wavenumber of 400–4000 cm⁻¹ were recorded using a

Perkin-Elmer spectrometer. X-ray photoelectron spectroscopy (XPS) was performed to determine the elemental composition, empirical formula, chemical and electronic state of elements in NCs via a Thermo Scientific K-Alpha system with an Al K-alpha X-ray source and the ion source energy between 100 V and 3 keV for the survey (Narayanan et al. 2020).

To observe the surface morphology of the NCs by field-emission scanning electron microscopy (FE-SEM; Model: Hitachi S-4200), the samples were mounted on aluminum stubs and ion beam sputter-coated with platinum for analysis with secondary electron detectors at an operating voltage of 10 kV. The elemental composition was analyzed using energy-dispersive X-ray spectroscopy (EDS) attached to FE-SEM. In the field-emission transmission electron microscopy (FE-TEM), a carbon-coated copper grid was dipped into the synthesized Ag-TiO₂ NC solution and dried at room temperature before analysis. The morphology of NCs was observed using FE-TEM (FEI Tecnai G2 F20, Hillsboro, Oregon, USA) at an accelerating voltage of 200 kV, and the selected area electron diffraction (SAED) pattern was also recorded. The elemental analysis was performed using high-angle annular dark-field scanning TEM (HAADF-STEM) and STEM-EDS with a point resolution of 0.24 nm, and a Cs of 1.2 mm using the EDS detector with an ultrathin window cooled with liquid nitrogen.

2.5. Photocatalytic degradation of an azo dye

To assess the photocatalytic degradation, Ag-TiO₂ (3:0.5, 3:1, and 3:1.5) NCs were used as photocatalysts towards the degradation of methylene blue (MB) as a model azo dye pollutants using a tungsten halogen lamp (400 W; 3 M, USA) as a light source ($\lambda > 500$ nm) and an irradiation intensity of 31 mW/cm² (Bagheri et al., 2014; Balu et al., 2018). Briefly, the experimental system containing 0.01% (w/v) of Ag-TiO₂ NCs with MB (10 mg/L) was put under dark for adsorption–desorption equilibrium for 30 min. Later, it was subjected to visible light irradiation at room temperature, and the degradation was monitored at different intervals using a UV–vis spectrophotometer (Shimadzu, model: UV-2600). The concentration of MB dye was quantified spectrophotometrically by measuring the absorbance at 663 nm.

2.6. Antibacterial activity of Ag-TiO₂ NCs

The antibacterial activity of Ag-TiO₂ NCs was evaluated using the agar well diffusion assay (Narayanan et al., 2021). For agar well diffusion assay, pure cultures of *S. aureus* and *E. coli* bacteria were cultured in MH agar plates, and a single bacterial colony was picked and grown in MH broth in a shaking incubator at 37 °C and 200 rpm until the optical density (O.D.) at 600 nm reached 0.8. These bacterial suspensions were used to spread plate onto MH agar plates. Later, a sterile cork-borer (8 mm) was used to make agar wells, and different Ag-TiO₂ NCs (5 mg; 40 mg/mL) were loaded into the wells and incubated at 37 °C for overnight. Ampicillin (200 μ g; 200 mg/mL) was used as a positive control. The diameter of the zone of inhibitions (ZOIs) was measured to find the antibacterial properties of NCs. The experiment was done in triplicates and the mean diameter was calculated.

3. Results

3.1. Green synthesis of Ag-TiO₂ nanocomposites

The formation of Ag-NPs on the surface of TiO₂-NPs to produce Ag-TiO₂ NCs was synthesized using an environmentally friendly green method without any toxic chemicals. The presence of phenylpropanoids and isoflavonoids (caffeic acid, chlorogenic acid, quercetin-3-O-rutinoside, and kaempferol-3-O-rutinoside), coumarins, lignans, and other metabolites in GB fruit extract gives antioxidant capacity for the reduction process and in the stabilization of NCs. In particular, the presence of polyphenols (enol form) such as quercetin, caffeic acid, and coumarins gives electrons to silver ions forming Ag⁰ NPs with the consequent oxidation of polyphenols forming quinone groups (keto form) (Fig. 1).

3.2. Optical, structural, and morphological characterizations of Ag-TiO₂ NCs

To investigate the absorbance bands of bare TiO₂-NPs and Ag-TiO₂ NCs, UV-vis absorption spectra were measured over the wavelength range of 200–800 nm at room temperature. The absorption spectra of different Ag-TiO₂ NCs (3:0.5; 3:1 and 3:1.5) have broad absorption spectra in the range of 250–600 nm, and their absorbance intensity was stronger than bare TiO₂-NPs. The whitish color of the bare TiO₂ suspension was changed to a brownish color solution indicating the formation of Ag-NPs on TiO₂-NPs by active molecules present in the extract. Moreover, these NCs displayed a broad surface plasmon resonance (SPR) band in the range of 350–600 nm, which is the characteristic of Ag-NPs with λ_{max} at 436.5, 428.5, and 422.8 nm for 3:0.5, 3:1, and 3:1.5 Ag-TiO₂ NCs, respectively (Fig. 2a). The bandgap energy of synthesized NCs was calculated using the following equation: $\alpha h\nu = A(h\nu - E_g)^n$; where E_g is the bandgap energy, α is the absorption coefficient, n corresponds to the nature of the transition, and A is a constant, which depends on the transition probability i.e., direct, or indirect (Yu et al., 2005). The bandgap energy of bare TiO₂-NPs and Ag-TiO₂ NCs has been calculated by extrapolating the lin-

ear portion of the plot of $h\nu$ versus $(\alpha h\nu)^2$ to the energy axis at $\alpha = 0$ (Fig. 2b). Compared to the bandgap of bare TiO₂-NPs (3.23 eV), bandgaps of 3:0.5 (2.63 eV), 3:1 (2.49 eV), and 3:1.5 (2.39 eV) Ag-TiO₂ NCs were reduced significantly by shifting to the visible range, which confirms the formation of Ag-NPs on the surface of TiO₂-NPs thereby reducing bandgap energy (Di Valentin and Pacchioni, 2013).

Fig. 3a displays the XRD patterns, which confirms the successful formation of Ag-NPs throughout the surface of TiO₂-NPs as well as the overall formation of Ag-TiO₂ NCs with crystalline nature. The diffraction peaks of bare TiO₂-NPs at 2θ values of 25.1°, 37.6°, 47.9°, 53.7°, 54.5° and 62.7°, which correspond to (101), (004), (200), (105), (211) and (204), respectively indicating the formation of crystal planes of anatase TiO₂ (JCPDS file No. 21–1272) (Pookmanee and Phanichphant, 2009). The peaks (111), (200), (220) and (311) at 38.05°, 44.21°, 64.38° and 77.34° 2θ , respectively present in the Ag-TiO₂ NCs are characteristics of face-centered cubic (fcc) crystalline nature of Ag-NPs (JCPDS file No. 4–783) (Khan et al., 2013), which confirms the deposition of Ag-NPs throughout the TiO₂-NPs surface. The average crystallite sizes of Ag-NPs were 8.1 ± 3.8 , 9.2 ± 2.9 , and 11.9 ± 3.0 nm for 3:0.5, 3:1, and 3:1.5 Ag-TiO₂ NCs, respectively.

The FT-IR measurements were performed to investigate the functional groups present on Ag-TiO₂ NCs that are involved in the capping and stabilization of NCs (Fig. 3b). FTIR spectra of bare TiO₂-NPs and GB fruit extract-derived Ag-TiO₂ NCs displayed the broad peak at 3308 cm⁻¹, which is associated with O–H stretching vibration, and the sharp peak around 1647 cm⁻¹ was characteristic of the deformation vibration of the physisorbed water molecules on the TiO₂ layer (Chuang and Chen, 2009). Moreover, C–H stretching vibrations in the epoxy were detected at 1069 cm⁻¹, and the peaks at 2927 and 1058 cm⁻¹ correspond to the C–H and C–O–H groups of ethanol adsorbed on the surface of TiO₂-NPs. FT-IR spectrum of GB extract is shown in Fig. S1. The spectral peak at 3270 cm⁻¹ was associated with the stretching vibration of hydroxyl (O–H) groups, 2923 cm⁻¹ peak corresponded to the C–H stretching of CH₂ groups, and the peak at 1587 cm⁻¹ corresponded to amide II. The peaks in the region of 1400–1200 cm⁻¹ were due to O–C–H, C–C–H, and C–O–H

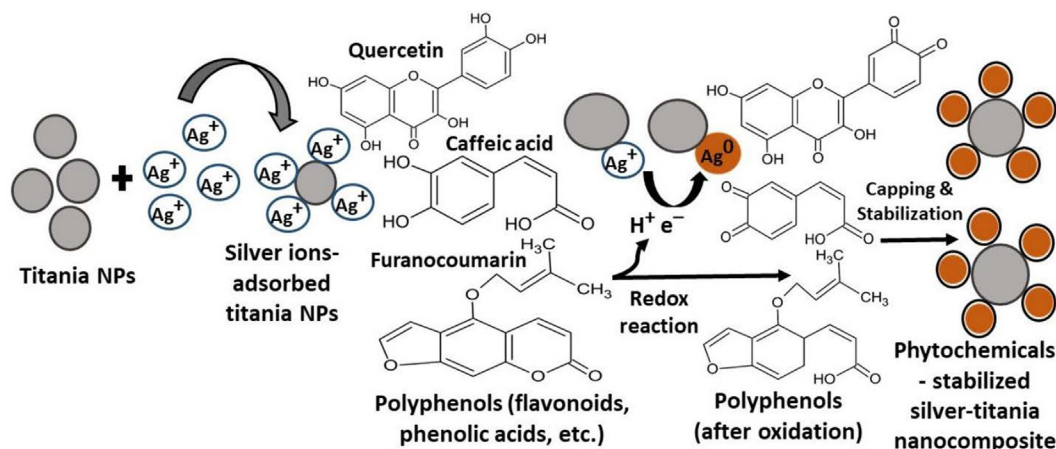


Fig. 1 Schematic diagram showing the mechanistic aspect of Ag-TiO₂ NCs synthesis by goji berry extract.

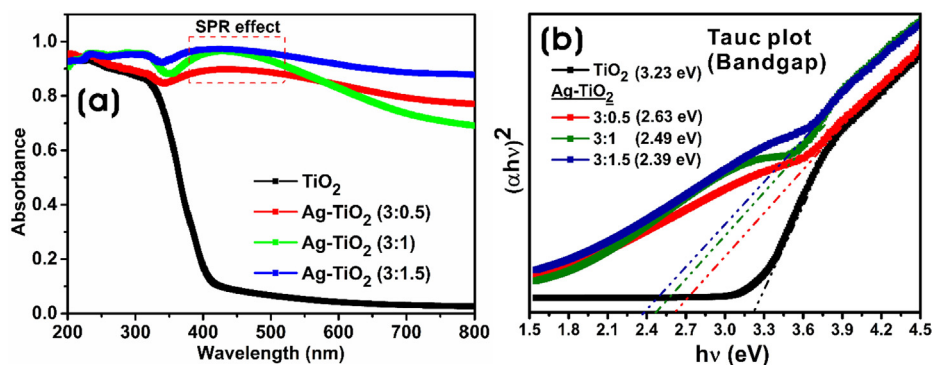


Fig. 2 (a) UV-vis absorption spectra, and (b) optical bandgap energy plot of bare TiO₂-NPs and Ag-TiO₂ NCs (3:0.5, 3:1, and 3:1.5).

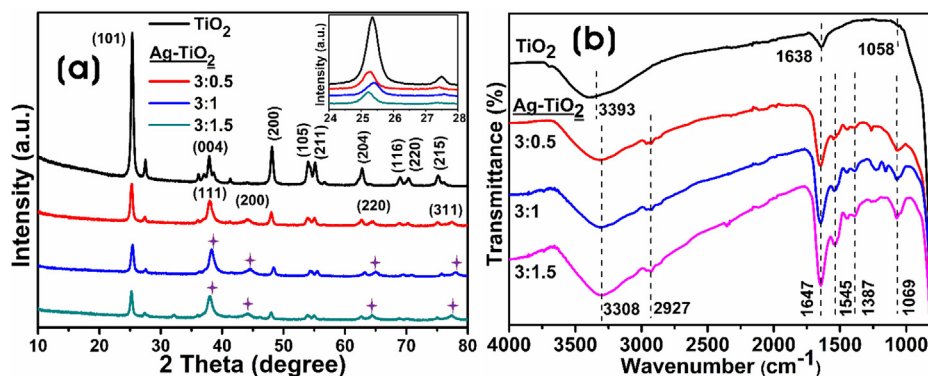


Fig. 3 (a) XRD analysis (inset shows the magnified portion of the (101) plane), and (b) FT-IR spectra of the bare TiO₂-NPs and Ag-TiO₂ NCs (3:0.5, 3:1, and 3:1.5).

bending vibrations of the carbohydrates, and the peaks in the region of 1150–900 cm⁻¹ were attributed to the stretching of C–O, and C–C bonds (Santos et al., 2019).

Fig. 4a shows the survey spectra and high-resolution spectra of Ag 3d, Ti 2p, and O 1s orbitals. From Fig. 4, it is clear that the bare TiO₂-NPs showed Ti 2p, O 1s, and C 1s elements, whereas Ag-TiO₂ (3:1) NC contains Ag 3d along with Ti 2p, O 1s, and C 1s elements. The peak for C 1s was ascribed to the carbon from macromolecules/metabolites of GB extract involved in the processes of reduction and stabilization of NCs. The high-resolution spectrum of Ag 3d peak in the Ag-TiO₂ NC (3:1) shows the binding energy (BE) matching to that of Ag 3d_{5/2} peak at 367.6 eV, indicating the formation of metallic silver. Besides, the BE of Ag 3d_{3/2} peak was observed at 373.6 eV (Fig. 4b). The Ag 3d spectrum of silver metal has well separated spin-orbit components, and the difference of BEs between Ag 3d_{5/2} and 3d_{3/2} peaks was 6.0 eV, which was characteristic of silver metal (Xiang et al., 2010). Fig. 4c shows the Ti 2p_{3/2} and Ti 2p_{1/2} peaks of bare TiO₂-NPs with BEs at 458.38 and 464.16 eV, respectively. After the formation of Ag-NPs onto the TiO₂-NPs surface, the formed Ag-TiO₂ NC (3:1) exhibited a shift in the BEs of Ti 2p_{3/2}, and Ti 2p_{1/2} peaks to 458.57 and 464.28 eV, respectively. Similarly, Fig. 4d shows the O1s peak with shifted BE from 529.98 to 529.78 eV in NCs. These changes in BE suggest that Ag-TiO₂ NCs were successfully synthesized. The SEM-EDX images of bare TiO₂-NPs and different Ag-TiO₂ NCs

are shown in Fig. S2. The results show spherical nanoparticles with slight aggregation, and there was a homogeneous and dense capping agent on Ag-TiO₂ NCs. However, the Ag-NPs were not uniformly deposited on the surface of TiO₂-NPs as reported previously (Behnajady et al., 2008). The elemental composition of TiO₂-NPs and Ag-TiO₂ NCs was determined by energy-dispersive X-ray spectroscopy (EDS) analysis. From EDS analysis, it is observed that the strong peaks appeared for Ti, Ag, and O elements confirming the formation of Ag-TiO₂ NCs.

Fig. 5 shows the FE-TEM images and SAED patterns of Ag-TiO₂ NCs (3:0.5, 3:1, and 3:1.5). The dark spots in FE-TEM images show the formation of Ag-NPs on the surface of TiO₂-NPs. The synthesized Ag-TiO₂ NCs were predominantly spherical in morphology with quasi-spherical and hexagonal Ag-NPs were decorated on the surface of TiO₂-NPs along with capping agents, which has been in concurrence with the previous reports (Kalathil et al., 2012) (Fig. 5a-f). The sizes of NCs calculated using the FE-TEM images showed that there was an increase in the particle size of Ag-NPs on TiO₂-NPs with an increase in the concentration of silver reactant. Ag-TiO₂ NC (3:0.5) had Ag-NPs in the range of 7.3–15.9 nm with an average of 11.2 ± 3.05 nm on the TiO₂-NPs surface, whereas 14.2–18.9 nm with an average of 15.8 ± 2.4 nm, and 13.1–23.0 nm with an average of 16.4 ± 4.5 nm were observed for 3:1 and 3:1.5 Ag-TiO₂ NCs, respectively.

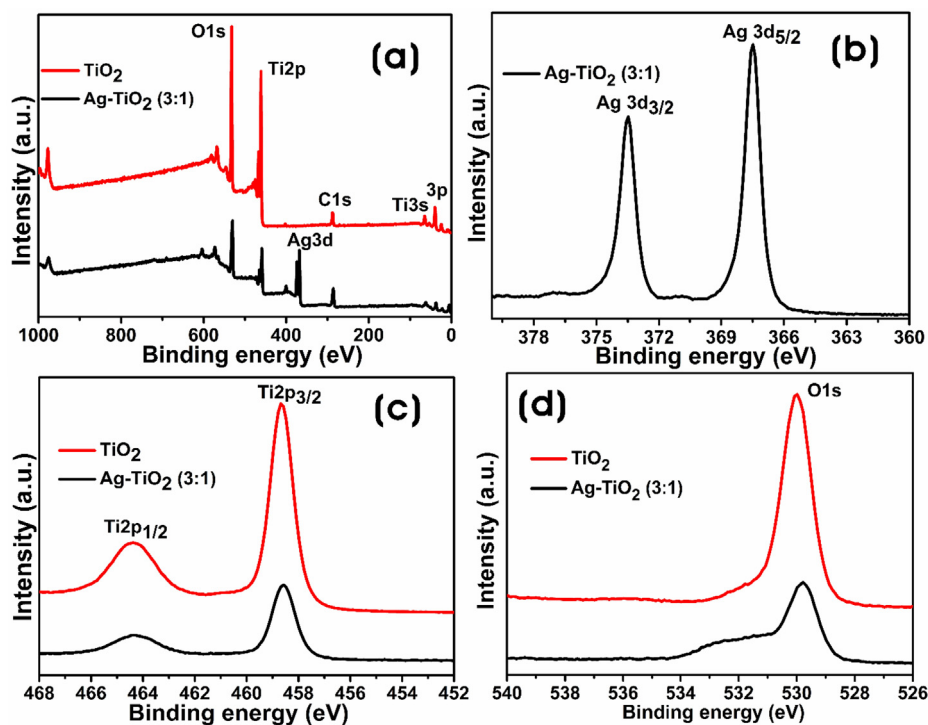


Fig. 4 XPS spectra of the bare TiO_2 -NPs and Ag-TiO_2 NC (3:1). (a) Survey spectra, (b) Ag 3d peak, (c) Ti 2p peak, and (d) O 1 s peak.

SAED patterns of TiO_2 of different NCs clearly show well-resolved diffraction rings, which are indicative of their polycrystallinity nature (Fig. 5c, 5f, and 5i). Element mapping analysis of the FE-TEM image shows the presence of Ag, Ti, and O elements in Ag-TiO_2 NCs (Fig. 6).

3.3. Applications of Ag-TiO_2 NCs

3.3.1. Photocatalytic degradation of MB by Ag-TiO_2 NCs

Interestingly, the higher photocatalytic activity was obtained under the experimental conditions with all the Ag-TiO_2 (3:0.5, 3:1, and 3:1.5) NCs (Fig. 7). Fig. 7a shows the photocatalytic degradation (C_t/C_0) as a function of the time, where C_t is the concentration of the dye (MB) at the time “t”, and C_0 is the initial concentration. In the absence of NCs, control experiments were performed, and there was no sufficient photocatalytic degradation of MB.

In the present work, all Ag-TiO_2 NCs as photocatalysts showed $> 90\%$ of photocatalytic degradation of MB in 130 min of visible light irradiation (Fig. 7a). Each experimental system containing MB dye solution (10 mg/L) and 0.01% (w/v) photocatalyst was left under dark for 30 min for the adsorption-desorption equilibrium, and the results showed the adsorption of 15–18% of MB dye on the Ag-TiO_2 NCs (Fig. 7b). Firstly, 3:0.5 and 3:1 Ag-TiO_2 NCs were assessed for the photocatalytic degradation of MB, which reached nearly $\sim 23\%$ and 24% , respectively, in 10 min after exposure to light. Thereafter, at every 15 min, the sample was taken and spectrophotometrically analyzed, which showed the time-dependent catalytic degradation of MB by NCs. More than $\sim 50\%$ of MB degradation occurred in 70 and 55 min

by 3:0.5 and 3:1 Ag-TiO_2 NCs, respectively, and finally, 90.7% and 93.4% degradation occurred in 130 min of visible light irradiation (Table 1). In contrast, the degradation efficiency of MB by Ag-TiO_2 NC (3:1.5) was marginally lower (91.8%) than Ag-TiO_2 NC (3:1), but slightly higher than Ag-TiO_2 NC (3:0.5) (Fig. 7b). In the absence of catalyst, the photolysis of MB was 9.4%, whereas bare TiO_2 -NPs degraded 73.4% of MB, respectively after 150 min of visible irradiation (Fig. S3). Fig. 8 represents the photoinduced charge separation, charge transfer, and photocatalytic degradation of dyes using Ag-TiO_2 NCs as photocatalyst under visible light irradiation.

3.3.2. Antibacterial assay

The antibacterial activity of green synthesized Ag-TiO_2 NCs (5 mg; 40 mg/mL) was evaluated using the agar well diffusion method. Fig. 9 shows the antibacterial activity of all Ag-TiO_2 NCs against *S. aureus* (Gram-positive) and *E. coli* (Gram-negative). TiO_2 -NPs were inert for both Gram-positive as well as -negative bacterial species. However, different Ag-TiO_2 NCs exhibited different levels of antimicrobial activity against bacteria. The zone of inhibitions (ZOIs) for *S. aureus* were 9.6 ± 0.57 and 12 ± 1.0 mm for 3:1 and 3:1.5 Ag-TiO_2 NCs, respectively, whereas ZOI for *E. coli* was 9.3 ± 0.57 mm for 3:1.5 Ag-TiO_2 NC. The ZOIs of ampicillin (positive control) were 29.3 ± 1.53 and 14 ± 1.0 mm for *S. aureus* and *E. coli*, respectively (Fig. 9). The goji berry plant extract (100 μl ; 2.8 mg/mL) did not produce any significant antibacterial activity against both Gram-positive and -negative bacteria (Fig. S4). Thus, Ag-TiO_2 NC (3:1.5) exhibited broad-spectrum antibacterial properties against both Gram-positive and -negative microorganisms.

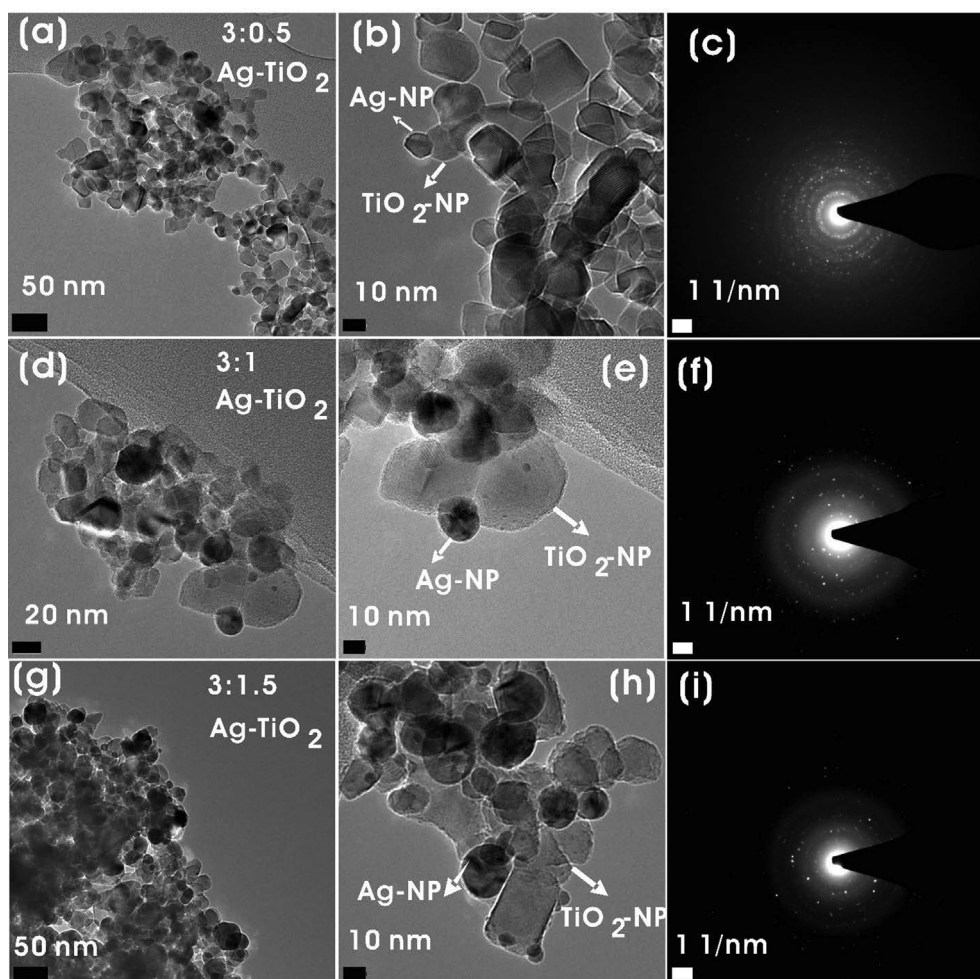


Fig. 5 FE-TEM images of (a,b) 3:0.5, (d,e) 3:1, and (g,h) 3:1.5 Ag-TiO₂ NCs. SAED images of (e) 3:0.5, (f) 3:1, and (i) 3:1.5 Ag-TiO₂ NCs.

4. Discussion

Green syntheses of nanocomposites using the extracts of plant materials such as stem, leaves, flowers, or fruits are usually safe. The synthesis method uses an environment-friendly solvent, non-hazardous and non-toxic reducing and stabilization agents. Many researchers have greatly exploited the natural resources for the green and sustainable synthesis of several nanocomposites in an environment-friendly method. Among several methods, a greener method using plant materials is advantageous as it is predominant with secondary metabolites, biomacromolecules, and other reducing agents with electron-shuttling compounds (Narayanan and Sakthivel, 2011; Patsilinakos et al., 2018). The red goji berries are rich in phytochemicals, minerals, carotenoids, 2-O- β -glucopyranosyl-L-ascorbic acid (AA-2 β G), and fatty acid composition. The presence of many bioactive compounds with high antioxidant ability can act as reducing agents in the formation of nanoparticles with unique shapes and morphologies (Ilic et al., 2020). The optical properties of NCs are dependent on the particle size and the surrounding environment. SPR is the resonant oscillation of valence electrons by incident light due to which nanoscale particles exhibit different colors. UV-vis spectra

also give information about the aggregation of nanoparticles. The increase of the concentration of AgNO₃ added to bare TiO₂-NPs from 0.5 to 1.5 mM, resulted in higher intensity of SPR absorption peak suggesting the reduction of silver ions to increased Ag-NPs and the formation of many NPs on the surface of TiO₂-NPs. Moreover, all NCs exhibited weak and broad SPR bands suggesting the formation of Ag-NPs with broader size distributions (Ider et al., 2017). As seen in Fig. 2b, the incorporation of Ag-NPs into the surface of TiO₂ resulted in the reduction of bandgap energy. The decrease in bandgap energy with an increase in the Ag-NPs on the surface of TiO₂ shows a redshift of the absorption peak and decreases the recombination rate of photoinduced electrons and holes and enhances photocatalytic activity (Gupta et al., 2013). Barone et al., (2014) also demonstrated a decrease in the optical bandgap from about 3 eV of TiO₂ to about 1.4 eV with the addition of silver to the TiO₂-NPs. The decrease in optical band explains the quenching of photoluminescence and the changes in UV-visible absorption due to the metallization of samples by the formation of Ag-NPs on the surface. The decoration of TiO₂ with metal/nonmetals or metal-nonmetal combinations reduces its bandgap and allows for the activation by visible light (Malati and Wong, 1984).

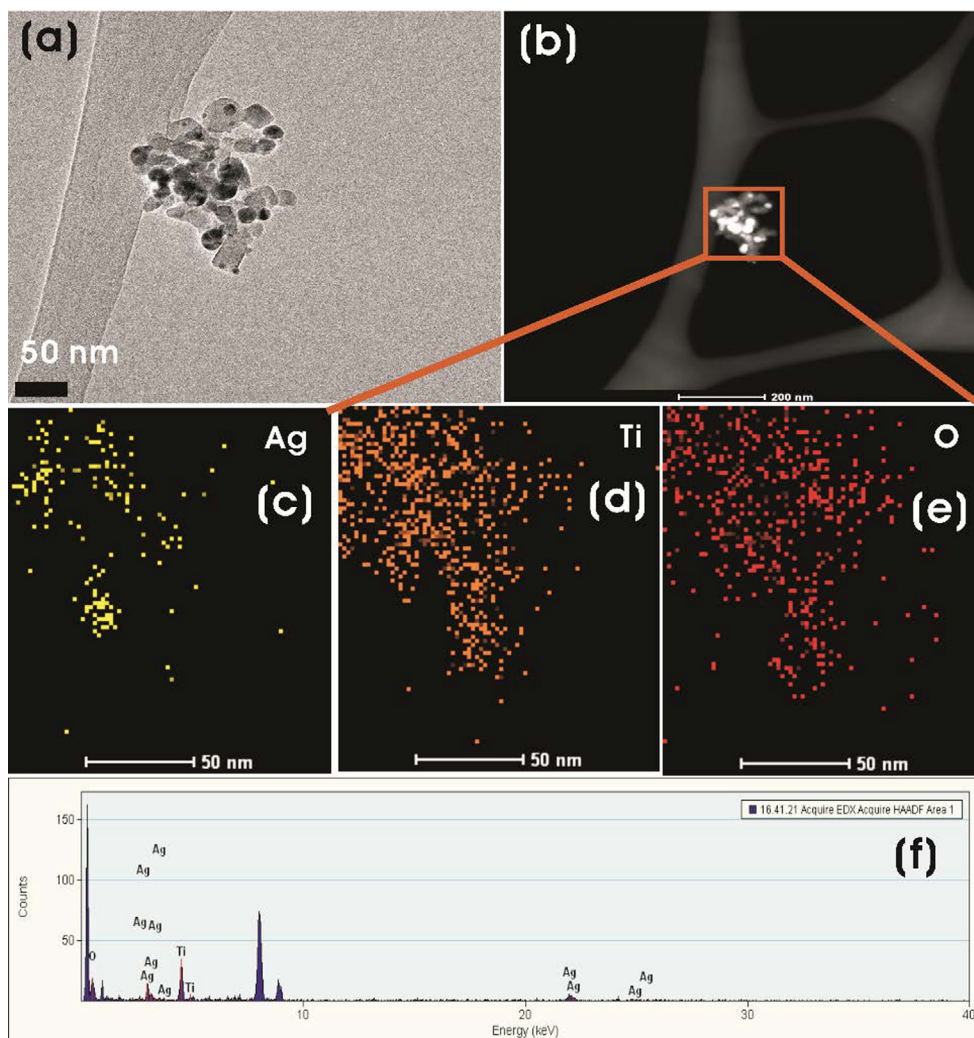


Fig. 6 (a) FE-TEM and (b) HAADF-STEM images of Ag-TiO₂ NC (3:1). (c-e) EDS mapping of Ag, Ti, and O elements and (f) EDS spectrum of the plotted area of Ag-TiO₂ NC (3:1).

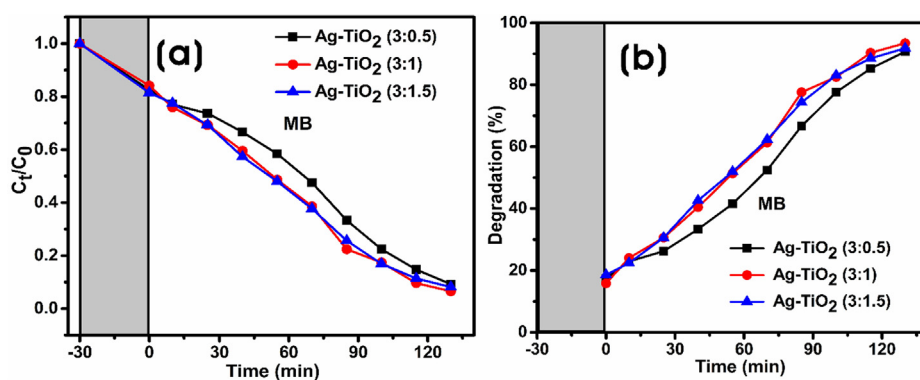


Fig. 7 Photocatalytic degradation of MB by Ag-TiO₂ NCs under visible light irradiation. (a) The plot of C_t/C_0 against time in the degradation of MB dye. (b) Degradation percentage (%) of MB against time.

The XRD analysis investigates the structures, phases, and crystal orientations of nanoparticles. XRD analysis showed that Ag-NPs have a face center cubic (fcc) structure impregnated on the surface of TiO₂-NPs. The unassigned

peaks in the spectra are due to the crystallization of biomacromolecules and metabolites from the GB extract on the surface of nanocomposites. Similar results were reported previously with biogenic Ag-NPs synthesis using the extracts of edible

Table 1 Green synthesis of Ag-TiO₂ NCs and their photocatalytic degradation of dyes and antibacterial activities

Plant extract	Irradiation	[Dye]	[Ag-TiO ₂]	Degradation (%)	Degradation time (min)	Pathogens	Reference
<i>Azadirachta indica</i>	UV	MB (0.01%) RB (0.01%)	0.2% (6% Ag) 0.2% (6% Ag)	97 90	120 120	–	(Saeed et al., 2019)
<i>Carpobrotus acinaciformis</i>	UV	MO (10 ppm)	0.01%	100	5	–	(Rostami-Vartoomi et al., 2016)
<i>Uncaria gambir</i> Roxb.	Solar	CR (10 ppm) RB (20 ppm)	0.01% 0.01%	100 99	19.5 120	–	(Wahyuni et al., 2019)
<i>Acacia nilotica</i>	–	–	–	–	–	<i>E. coli</i> , <i>C. albicans</i> , MRSA & <i>S. aureus</i>	(Rao et al., 2019)
<i>Origanum majorana</i>	–	–	–	–	–	<i>E. coli</i> , <i>B. subtilis</i> & <i>A. niger</i>	(Bhardwaj & Singh, 2021)
<i>Cestrum nocturnum</i>	Visible	MB (0.001%)	0.011%	90	40	<i>E. coli</i> & <i>P. aeruginosa</i>	(Tahir et al., 2016)
<i>Lycium barbarum</i> L.	Visible	MB (10 ppm)	0.01%	93.4	130	<i>E. coli</i> & <i>P. aeruginosa</i>	(This study)

MB – Methylene blue; RB – Rhodamine B; MO – Methyl orange.

mushroom and geranium leaves (Philip, 2009; Vanaja and Annadurai, 2013). The FT-IR measurement was performed to investigate the functional groups of the biomolecules in the GB fruit extract, which were involved in the reduction process to form Ag-NPs and responsible for the capping and stabilization processes to form Ag-TiO₂ NCs. Generally, the phenolic groups, aromatic amines, amide (I) groups, and secondary alcohols in the plant extracts interact with the surface of metal NPs for reduction and stabilization (Kumar et al., 2020; Kabir et al., 2020). The oxidation/reduction property of flavonoids and isoflavonoids (caffeic acid, chlorogenic acid, quercetin-3-O-rutinoside, and kaempferol-3-O-rutinoside) present in the fruit extract plays an important role in the synthesis of Ag-NPs on the TiO₂-NPs surface (Rasineni et al., 2008).

XPS is a powerful quantitative technique to elucidate the electronic structure and elemental composition of nanomaterials with their oxidation states. In our study, the surface composition, and chemical states of bare TiO₂-NPs and Ag-TiO₂ NCs were carried out by XPS analysis. FE-SEM images and EDS spectra of synthesized Ag-TiO₂ NCs have been used to characterize the information on the surface morphology and elemental composition. The occurrence of separate elemental signals for silver, titanium, and oxygen suggests that silver ions are successfully integrated into the TiO₂ lattice. The increase of silver intensity shows the increased formation of Ag-NPs on the TiO₂ surface, which is in concurrence with the previous reports (Ali et al. 2018; Sobana et al., 2006). FE-TEM was used to examine the dispersion, size, and shape of Ag-TiO₂ NCs prepared using GB extract. The average size of Ag-NPs formed on TiO₂-NPs increased with the concentration of AgNO₃ from 0.5 to 1.5 mM. A possible reason for increasing NPs size can be due to the lack of extract components with higher AgNO₃ concentration to cap the surface of NPs, which leads to low thermodynamic stability and subsequent agglomerate over time leading to the formation of quasi-spherical and hexagonal shapes of Ag-NPs on the surface of TiO₂-NPs (Ahmad et al., 2018). SAED patterns of concentric bright circular rings resulted from the orientation of crystal planes confirming the crystalline nature of TiO₂. The presence of rings is due to the random orientation of the nanocrystallites, and the brightness of circular rings suggests the polycrystalline nature of TiO₂ (Mourdikoudis et al., 2018).

Azo dyes are organic compounds that constitute two-third of all synthetic dyes used in the textile dyeing and pharmaceutical industries. Many azo dyes are carcinogenic/mutagenic and provoke allergic reactions. The toxicity of these dyes is mainly because of the presence of many benzene rings in their structure. The products of many degraded dyes also impose carcinogenicity, for instance, benzidine, which is a cleaved product of many azo dyes, is a known carcinogen for the human urinary bladder (Gicevic et al., 2020). The photocatalytic property of a nanocomposite in the degradation of dyes by visible light irradiation is the ability to produce photogenerated electrons by the SPR effect. However, the photocatalytic degradation by bare TiO₂-NPs was lower and occurred under harsh conditions (Sobana et al., 2006). The improved absorption behavior of Ag-TiO₂ NCs compared to bare TiO₂-NPs in the visible light region was employed as a photocatalyst in the degradation of azo dyes. This excellent degradation ability of Ag-TiO₂ NCs towards MB was mainly attributed to the characteristic SPR phenomena of Ag-NPs, the tuning bandgap, and the surface properties of photocatalysts (Sarina et al.,

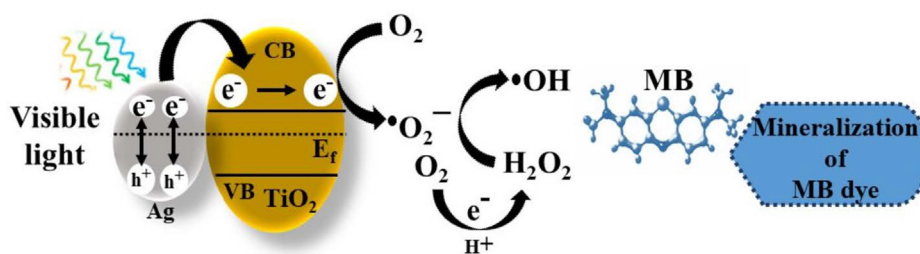


Fig. 8 Schematic illustration of the possible mechanism for the photocatalytic degradation of MB dye by Ag-TiO₂ NCs.

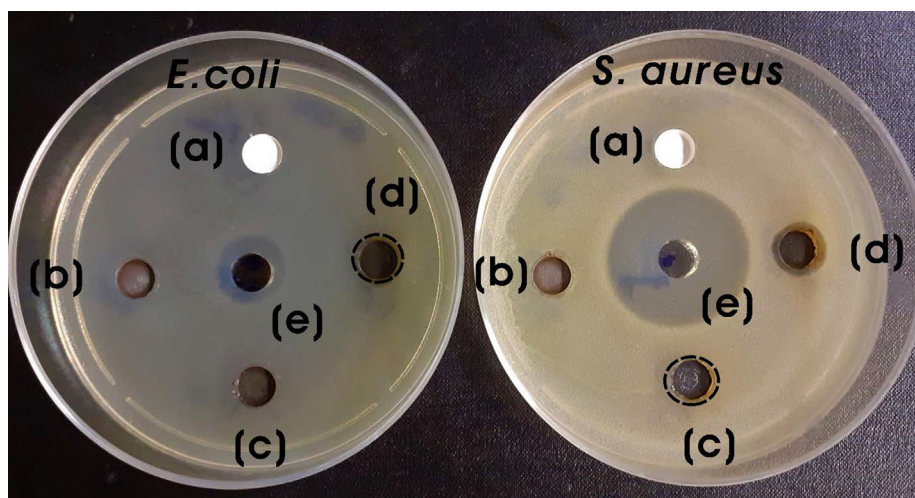


Fig. 9 Photographs of ZOIs for (a) bare TiO₂-NPs, (b) 3:0.5, (c) 3:1, and (d) 3:1.5 Ag-TiO₂ NCs (5 mg; 40 mg/mL) and (e) positive control (ampicillin, 200 µg; 200 mg/mL) against *S. aureus* and *E. coli*.

2013). In 2017, Rather and colleagues demonstrated that the plasmonic metal (Cu, Au, and Ag)-TiO₂ NCs was effectively used as photocatalyst for photooxidative decomposition of MB resulting in the complete photomineralization to carbon dioxide (CO₂) and water in comparison to TiO₂ (Rather et al., 2017). Even, the green synthesized Ag-NPs using the stem extract of *Nepeta leucophylla* exhibited plasmon-induced photocatalytic degradation of MB (82.8%) in 180 min under visible light (Singh and Dhaliwal, 2020). Recently, the nano-sized Fe₂Zr_{0.85}W_{0.15}O₇ system showed promising photocatalytic degradative activity of MB in real textile wastewater with pseudo-first-order kinetics at the optimum degradation conditions of 1.5 g/L catalyst at pH 11.0 (Abbas et al., 2020). These green synthesized Ag-TiO₂ NCs-based photocatalysts have shown immense prospectives for wastewater treatment applications, as it requires a low amount of photocatalyst and efficient degradation of MB under visible light irradiation. The UV-irradiation of Ag-TiO₂ prepared using *Azadirachta indica* leaf extract for the degradation of MB and rhodamine B (RB) dyes showed that >90% of dyes were degraded in 120 min. (Saeed et al., 2019). The solar light irradiation of RB with Ag/TiO₂ NC synthesized using *Uncaria gambier* Roxb. leaf extract showed 99% degradation at 120 min (Wahyuni et al., 2019). In another instance, the immobilization of Ag-NPs on TiO₂ surface using the extract of *Carpobrotus acinaciformis* showed photocatalytic degradation of methyl orange (MO) and CR than bare TiO₂-

NPs as photocatalyst (Rostami-Vartooni et al., 2016). The Ag/TiO₂ NC prepared using the leaf extract of *Cestrum nocturnum* showed visible light photocatalytic degradation of MB as well as visible light photoinhibition of *E. coli* and *P. aeruginosa* (Tahir et al., 2016).

On visible light irradiation, the electrons from the valence band (VB) of silver are injected rapidly into the conduction band (CB) of the TiO₂ by the SPR effect, and Ag is converted to Ag⁺ ions. These injected electrons on the TiO₂ react with the dissolved molecular oxygen molecules (O₂) in water to produce reactive species, such as [•]O₂⁻ (superoxide) and hydrogen peroxide H₂O₂ in oxygen-equilibrated solution. These reactive species can interact to produce [•]OH (hydroxyl) radicals, which effectively degrades dye molecules and contaminants to various products (Varma et al., 2016; Yang et al., 2013). However, the size distribution of Ag-NPs on the NC plays a key role in determining the photocatalytic degradative efficiency of the nanocomposites (Kodom et al., 2015). Chen et al., (2014) demonstrated that the improved photocatalysis of silver-decorated TiO₂ nanotube arrays is attributed to the enhanced light-harvesting SPR effect of Ag-NPs. The changes in the photocatalytic ability of NCs are mainly due to the variations in the electron transport and separation of the plasmon-generated electrons and holes in the Ag-NPs in the NC. The formation of larger Ag-NPs on Ag-TiO₂ NC (3:1.5) showed lower photocatalytic activity due to the more scattering of visible light and excitation of fewer electrons, which are injected

into the conduction band of TiO₂ than that of smaller Ag-NPs on other NCs. As a result, the photocatalytic activity of larger Ag-NPs decorated TiO₂ NC is muted in comparison to other NCs.

Metals exhibit strong antibacterial activity against pathogenic microorganisms, *in-situ* generated silver and copper bimetallic (Ag/Cu) nanoparticles on cotton fabrics using the extracts of red sanders powder or aloe vera showed antibacterial activities against bacteria for applications, such as antibacterial bed and dressing materials (Gollapudi et al., 2020; Mamatha et al., 2020; Venkateswara Rao et al., 2019). Similarly, various metal nanocomposites (Ag-TiO₂ NCs) also exhibited broad-spectrum antibacterial properties against both Gram-positive and -negative microorganisms (Noreen et al., 2019). The differences in the antibacterial activity of NCs between Gram-positive and gram-negative bacteria are primarily due to the differences in their membrane structure and the thickness of the peptidoglycan layer (Kim et al., 2007; Sapkota et al., 2018). Ag-NPs have been previously reported to kill microbes for many decades (Allafchian et al., 2016). Thus, the immobilization of Ag-NPs on TiO₂-NPs (Ag-TiO₂ NCs) acts as an efficient antibacterial photocatalytic nanomaterial. Generally, the antibacterial effect of Ag-NPs is due to the release of silver ions, which react with the thiol group (-SH) of proteins leading to bacterial inactivation and death. These silver ions have also been reported to uncouple the respiratory electron transport chain (ETC) from oxidative phosphorylation by inhibiting the enzymes in the respiratory chain or by interfering with membrane permeability (Qing et al., 2018). In addition, the formation of strong oxidizing agents by TiO₂-NPs disrupts the outer and cytoplasmic bacterial membranes by lipid peroxidation leading to the death of microbes (Maness et al., 1999). Rao et al., (2019) demonstrated the antimicrobial activity of spherical Ag-TiO₂ NPs synthesized using the aerial extract of *Acacia nilotica* plant against pathogenic microorganisms in the order of *E. coli* > *Candida albicans* > methicillin-resistant *S. aureus* (MRSA) > *Pseudomonas aeruginosa*. Similarly, Ag-TiO₂ NCs synthesized using the leaf extract of *Origanum majorana* also showed significant antimicrobial activity against *E. coli*, *Bacillus subtilis*, and *Aspergillus niger* (Bhardwaj and Singh, 2021). In this study, Ag-TiO₂ NC (3:1.5) shows significant activity against *S. aureus* than *E. coli*, whereas Ag-TiO₂ NC (3:1) shows marginal inhibition. It is noteworthy to mention that Ag-TiO₂ NC (3:1.5) significantly affects the permeability of both Gram-positive (*S. aureus*) and -negative (*E. coli*) bacteria. However, *E. coli* is less permeable to released silver ions from NC when compared with *S. aureus* (Feng et al., 2000).

5. Conclusions

In summary, we demonstrated an environmentally friendly method to prepare Ag-TiO₂ NCs using the aqueous extract of goji berries without any added chemicals at room temperature. The synthesized Ag-TiO₂ NCs were characterized by UV-vis, XRD, FTIR, XPS, SEM, and FE-TEM analyses. The photocatalytic property of Ag-TiO₂ NCs was highly pronounced than bare TiO₂-NPs due to the efficient interfacial interaction between silver and titania nanoparticles leading to the charge separation as well as the transfer of photogenerated charge carrier under visible light irradiation. The

enhanced photocatalytic activities of Ag-TiO₂ NC (3:1) could be attributed to the enhanced SPR effect of Ag-NPs that have the better light-harvesting property with improved plasmon-generated electrons. The present approach not only provides an efficient green method of synthesizing the metal-decorated TiO₂ nanocomposites but also provides an eco-friendly photocatalyst for wastewater remediation and antibacterial applications. Overall, the green synthesized Ag-TiO₂ NCs using the fruit extract could be used as cost-effective, benign, sustainable, and effective photocatalysts in organic syntheses and wastewater treatments as well as antibacterial agents for various nanotechnological and biomedical applications.

CRedit authorship contribution statement

Abdulrahman Ahmed Sharwani: Conceptualization, Methodology, Validation, Formal analysis, Writing – original draft, Writing – review & editing. **Kannan Badri Narayanan:** Data analysis, Writing – Final draft, review & editing, Supervision. **Mohammad Ehtisham Khan:** Data analysis, Writing – review & editing. **Sung Soo Han:** Resources, Supervision.

Declaration of Competing Interest

The authors declare that they have no known competing financial interests or personal relationships that could have appeared to influence the work reported in this paper.

Acknowledgments

This work was supported by the King Abdullah Scholarship Program (2018), Ministry of Education, Saudi Arabia, and the Basic Science Research Program through the National Research Foundation of Korea (NRF) (#2019R111A3A01062440, #2020R1A2C1012586, & #2020R1A6A1A03044512) funded by the Korean Ministry of Education, Science and Technology. The authors thank the Core Research Support Center for Natural Products and Medical Materials (CRCNM) for instrumentation support.

Appendix A. Supplementary material

Supplementary data to this article can be found online at <https://doi.org/10.1016/j.arabjc.2021.103456>.

References

- Abbas, H.A., Nasr, R.A., Khalaf, A., Al Bawab, A.A., Jamil, T.S., 2020. Photocatalytic degradation of methylene blue by fluorite type Fe₂Zr_{2-x}W_xO₇ system under visible light irradiation. *Ecotoxicol. Environ. Saf.* 196, 110518.
- Ahmad, N, Ang, B.C., M.A., A., Bong, C.W., 2018. Influence of precursor concentration and temperature on the formation of nanosilver in chemical reduction method. *Sains Malays.* 47 (1), 157–168.
- Ahmed, S., Ahmad, M., Swami, B.L., Ikram, S., 2016a. A review on plants extract mediated synthesis of silver nanoparticles for antimicrobial applications: a green expertise. *J. Adv. Res.* 7 (1), 17–28.
- Ahmed, S., Saifullah, Ahmad, M., Swami, B.L., Ikram, S., 2016b. Green synthesis of silver nanoparticles using *Azadirachta indica* aqueous leaf extract. *J. Radiat. Res. Appl. Sci.* 9 (1), 1–7.

- Ali, T., Ahmed, A., Alam, U., Uddin, I., Tripathi, P., Muneer, M., 2018. Enhanced photocatalytic and antibacterial activities of Ag-doped TiO₂ nanoparticles under visible light. *Mater. Chem. Phys.* 212, 325–335.
- Allafchian, A., Jalali, S.A.H., Bahramian, H., Ahmadvand, H., 2016. Preparation, characterization, and antibacterial activity of NiFe₂O₄/PAMA/Ag–TiO₂ nanocomposite. *J. Magn. Magn. Mater.* 404, 14–20.
- Amini, N., Amin, G., Azar, Z.J., 2017. Green synthesis of silver nanoparticles using *Avena sativa* L. extract. *Nanomed. Res. J.* 2, 57–63.
- Aswathy Aromal, S., Philip, D., 2012. Green synthesis of gold nanoparticles using *Trigonella foenum-graecum* and its size-dependent catalytic activity. *Spectrochim. Acta A Mol. Biomol. Spectrosc.* 97, 1–5.
- Atarod, M., Nasrollahzadeh, M., Sajadi, S.M., 2016. Euphorbia heterophylla leaf extract mediated green synthesis of Ag/TiO₂ nanocomposite and investigation of its excellent catalytic activity for reduction of variety of dyes in water. *J. Colloid Interface Sci.* 462, 272–279.
- Bagheri, M., Mahjoub, A.R., Mehri, B., 2014. Enhanced photocatalytic degradation of congo red by solvothermally synthesized CuInSe₂-ZnO nanocomposites. *RSC Adv.* 4 (42), 21757. <https://doi.org/10.1039/c4ra011753f>.
- Bakbolat, B., Daulbayev, C., Sultanov, F., Beissenov, R., Umirzakov, A., Mereke, A., Bekbaev, A., Chuprakov, I., 2020. Recent developments of TiO₂-based photocatalysis in the hydrogel evolution and photodegradation: a review. *Nanomaterials* 10, 1790.
- Balu, S., Uma, K., Pan, G.-T., Yang, T., Ramaraj, S., 2018. Degradation of methylene blue dye in the presence of visible light using SiO₂@ α -Fe₂O₃ nanocomposites deposited on SnS₂ flowers. *Materials* 11 (6), 1030. <https://doi.org/10.3390/ma11061030>.
- Barone, P., Stranges, F., Barberio, M., Renzelli, D., Bonanno, A., Xu, F., 2014. Study of band gap of silver nanoparticles – titanium dioxide nanocomposites. *J. Chem.* 2014, 1–6.
- Behnajady, M., Modirshahla, N., Shokri, M., Rad, B., 2008. Enhancement of photocatalytic activity of TiO₂ nanoparticles by silver doping: photodeposition versus liquid impregnation methods. *Global NEST J.* 10, 1–7.
- Bhardwaj, D., Singh, R., 2021. Green biomimetic synthesis of Ag-TiO₂ nanocomposite using *Origanum majorana* leaf extract under sonication and their biological activities. *Bioresour. Bioprocess.* 8, 1.
- Camargo, P.H.C., Satyanarayana, K.G., Wypych, F., 2009. Nanocomposites: synthesis, structure, properties and new application opportunities. *Mater. Res.* 12 (1), 1–39.
- Chen, K., Feng, X., Tian, H., Li, Y., Xie, K., Hu, R., Cai, Y., Gu, H., 2014. Silver-decorated titanium dioxide nanotube arrays with improved photocatalytic activity for visible light irradiation. *J. Mater. Res.* 29 (11), 1302–1308.
- Chuang, H.-Y., Chen, D.-H., 2009. Fabrication and photocatalytic activities in visible and UV light regions of Ag@TiO₂ and NiAg@TiO₂ nanoparticles. *Nanotechnology* 20 (10), 105704. <https://doi.org/10.1088/0957-4484/20/10/105704>.
- Cozzoli, P.D., Fanizza, E., Comparelli, R., Curri, M.L., Agostiano, A., Laub, D., 2004. Role of metal nanoparticles in TiO₂/Ag nanocomposite-based microheterogeneous photocatalysis. *J. Phys. Chem. B* 108 (28), 9623–9630.
- Dhingra, R., Naidu, S., Upreti, G., Sawhney, R., 2010. Sustainable nanotechnology: through green methods and life-cycle thinking. *Sustainability* 2 (10), 3323–3338.
- Di Valentin, C., Pacchioni, G., 2013. Trends in non-metal doping of anatase TiO₂: B, C, N and F. *Catal. Today* 206, 12–18.
- Dong, C., Cao, C., Zhang, X., Zhan, Y., Wang, X., Yang, X., Zhou, K., Xiao, X., Yuan, B., 2017. Wolfberry fruit (*Lycium barbarum*) extract mediated novel route for the green synthesis of silver nanoparticles. *Optik* 130, 162–170.
- Fatimah, I.s., 2016. Green synthesis of silver nanoparticles using extract of *Parkia speciosa* Hassk pods assisted by microwave irradiation. *J. Adv. Res.* 7 (6), 961–969.
- Feng, Q.L., Wu, J., Chen, G.Q., Cui, F.Z., Kim, T.N., Kim, J.O., 2000. A mechanistic study of the antibacterial effect of silver ions on *Escherichia coli* and *Staphylococcus aureus*. *J. Biomed. Mater. Res.* 52 (4), 662–668.
- Gicevic, A., Hindija, L., Karacic, A., 2020. IFMBE Proceedings, Vol. 73: CMBEBIH 2019: Proceedings of the International Conference on Medical and Biological Engineering, 16–18 May 2019, B. Luka, A. Badnjevic, R. Skrbic, L.G. Pokvic, Eds. Sham: Springer Nature 581–587. https://doi.org/10.1007/978-3-030-17971-7_88.
- Gollapudi, V.R., Mallavarapu, U., Seetha, J., Akepogu, P., Amara, V. R., Natarajan, H., Anumakonda, V., 2020. *In situ* generation of silver and silver oxide nanoparticles on cotton fabrics using *Tinospora cordifolia* as bio reductant. *SN Appl. Sci.* 2, 508.
- Gudikandula, K., Charya Maringanti, S., 2016. Synthesis of silver nanoparticles by chemical and biological methods and their antimicrobial properties. *J. Exp. Nanosci.* 11 (9), 714–721.
- Gupta, K., Singh, R.P., Pandey, A., Pandey, A., 2013. Photocatalytic antibacterial performance of TiO₂ and Ag-doped TiO₂ against *S. aureus*, *P. aeruginosa* and *E. coli*. *Beilstein J. Nanotechnol.* 4, 345–351.
- Habibi, B., Hadilou, H., Mollaei, S., Yazdinezhad, A., 2017. Green synthesis of silver nanoparticles using the aqueous extract of *Prangos ferulaceae* leaves. *Int. J. Nano Dimens.* 8, 132–141.
- Ider, M., Abderrafi, K., Eddahbi, A., Ouaskit, S., Kassiba, A., 2017. Silver metallic nanoparticles with surface plasmon resonance: synthesis and characterizations. *J. Clust. Sci.* 28 (3), 1051–1069.
- Ilic, T., Dodevska, M., Marčetić, M., Božić, D., Kodranov, I., Vidović, B., 2020. Chemical characterization, antioxidant and antimicrobial properties of goji berries cultivated in Serbia. *Foods* 9 (11), 1614. <https://doi.org/10.3390/foods9111614>.
- Kabir, S.R., Asaduzzaman, AKM, Amin, R., Haque, ASM.T., Ghose, R., Rahman, M.M., Islam, J., Amin, M.B., Hasan, I., Debnath, T., Chun, B.-S., Zhao, XuDong, Rahman Khan, M.K., Alam, M.T., 2020. *Zizyphus mauritiana* fruit extract-mediated synthesized silver/silver chloride nanoparticles retain antimicrobial activity and induce apoptosis in MCF-7 cells through the Fas pathway. *ACS Omega* 5 (32), 20599–20608.
- Kalathil, S., Khan, M.M., Banerjee, A.N., Lee, J., Cho, M.H., 2012. A simple biogenic route to rapid synthesis of Au@TiO₂ nanocomposites by electrochemically active biofilms. *J. Nanopart. Res.* 14, 1–9.
- Khan, M.M., Ansari, S.A., Amal, M.I., Lee, J., Cho, M.H., 2013. Highly visible light active Ag@TiO₂ nanocomposites synthesized using an electrochemically active biofilm: a novel biogenic approach. *Nanoscale* 5 (10), 4427. <https://doi.org/10.1039/c3nr00613a>.
- Kikuchi, Y., Sunada, K., Iyoda, T., Hashimoto, K., Fujishima, A., 1997. Photocatalytic bactericidal effect of TiO₂ thin films: dynamic view of the active oxygen species responsible for the effect. *J. Photochem. Photobiol. A Chem.* 106 (1-3), 51–56.
- Kim, J.S., Kuk, E., Yu, K.N., Kim, J.-H., Park, S.J., Lee, H.J., Kim, S.H., Park, Y.K., Park, Y.H., Hwang, C.-Y., Kim, Y.-K., Lee, Y.-S., Jeong, D.H., Cho, M.-H., 2007. Antimicrobial effects of silver nanoparticles. *Nanomedicine* 3 (1), 95–101.
- Kodom, T., Rusen, E., Calinescu, I., Mocanu, A., Somoghi, R., Dinescu, A., Diacon, A., Boscornea, C., 2015. Silver nanoparticles influence on photocatalytic activity on hybrid materials based on TiO₂ P25. *Catal. Nanomater.* 2015, 210734.
- Kumar, H., Bhardwaj, K., Dhanjal, D.S., Nepovimova, E., Şen, F., Regassa, H., Singh, R., Verma, R., Kumar, V., Kumar, D., Bhatia, S.K., Kuča, K., 2020. Fruit extract mediated green synthesis of metallic nanoparticles: a new avenue in pomology applications. *Int. J. Mol. Sci.* 21 (22), 8458. <https://doi.org/10.3390/ijms21228458>.

- Malati, M.A., Wong, W.K., 1984. Doping TiO₂ for solar-energy applications. *Surf. Technol.* 22 (4), 305–322.
- Mamatha, G., Varada Rajulu, A., Madhukar, K., 2020. *In situ* generation of bimetallic nanoparticles in cotton fabric using aloe vera leaf extract, as a reducing agent. *J. Nat. Fibers* 17 (8), 1121–1129. <https://doi.org/10.1080/15440478.2018.1558146>.
- Maness, P.-C., Smolinski, S., Blake, D.M., Huang, Z., Wolfrum, E.J., Jacoby, W.A., 1999. Bactericidal activity of photocatalytic TiO₂ reaction: toward an understanding of its killing mechanism. *Appl. Environ. Microbiol.* 65 (9), 4094–4098.
- Martins, P., Kappert, S., Nga Le, H., Sebastian, V., Kühn, K., Alves, M., Pereira, L., Cuniberti, G., Melle-Franco, M., Lanceros-Méndez, S., 2020. Enhanced photocatalytic activity of Au/TiO₂ nanoparticles against ciprofloxacin. *Catalysts* 10 (2), 234. <https://doi.org/10.3390/catal10020234>.
- Mohammad, A., Karim, M.R., Khan, M.E., Khan, M.M., Cho, M.H., 2019. Biofilm-assisted fabrication of Ag@ SnO₂-g-C₃N₄ nanostructures for visible light-induced photocatalysis and photoelectrochemical performance. *J. Phys. Chem. C* 123 (34), 20936–20948.
- Mourdikoudis, S., Pallares, R.M., Thanh, N.T.K., 2018. Characterization techniques for nanoparticles: comparison and complementarity upon studying nanoparticle properties. *Nanoscale* 10 (27), 12871–12934.
- Narayanan, K.B., Kim, H.D., Han, S.S., 2020. Biocompatibility and hemocompatibility of hydrothermally derived reduced graphene oxide using soluble starch as a reducing agent. *Colloids Surf. B Biointerfaces* 185, 110579. <https://doi.org/10.1016/j.colsurfb.2019.110579>.
- Narayanan, K.B., Park, G.T., Han, S.S., 2021. Antibacterial properties of starch-reduced graphene oxide–polyiodide nanocomposite. *Food Chem.* 342, 128385. <https://doi.org/10.1016/j.foodchem.2020.128385>.
- Narayanan, K.B., Sakthivel, N., 2011. Green synthesis of biogenic metal nanoparticles by terrestrial and aquatic phototrophic and heterotrophic eukaryotes and biocompatible agents. *Adv. Colloid Interf. Sci.* 169 (2), 59–79.
- Natsuki, J., Natsuki, T., Hashimoto, Y., 2015. A review of silver nanoparticles: synthesis methods, properties and applications. *Int. J. Mater. Sci. Appl.* 4, 325–332.
- Ndikau, M., Noah, N.M., Andala, D.M., Masika, E., 2017. Green synthesis and characterization of silver nanoparticles using *Citrus lanatus* fruit rind extract. *Int. J. Anal. Chem.* 2017, 1–9.
- Noreen, Z., Khalid, N.R., Abbasi, R., Javed, S., Ahmad, I., Bokhari, H., 2019. Visible light sensitive Ag/TiO₂/graphene composite as a potential coating material for control of *Campylobacter jejuni*. *Mater. Sci. Eng. C* 98, 125–133.
- Patsilinakos, A., Ragno, R., Carradori, S., Petralito, S., Cesa, S., 2018. Carotenoid content of goji berries: CIELAB, HPLC-DAD analyses and quantitative correlation. *Food Chem.* 268, 49–56.
- Philip, D., 2009. Biosynthesis of Au, Ag and Au–Ag nanoparticles using edible mushroom extract. *Spectrochim. Acta A Mol. Biomol. Spectrosc.* 73 (2), 374–381.
- Pookmanee, P., Phanichphant, S., 2009. Titanium dioxide powder prepared by a sol-gel method. *J. Ceram. Process Res.* 10, 167–170.
- Qing, Y., Cheng, L., Li, R., Liu, G., Zhang, Y., Tang, X., Wang, J., Liu, H., Qin, Y., 2018. Potential antibacterial mechanism of silver nanoparticles and the optimization of orthopedic implants by advanced modification technologies. *Int. J. Nanomedicine* 13, 3311–3327.
- Venkateswara Rao, A., Ashok, B., Uma Mahesh, M., Venkata Subbareddy, G., Chandra Sekhar, V., Venkata Ramanamurthy, G., Varada Rajulu, A., 2019. Antibacterial cotton fabrics with *in situ* generated silver and copper bimetallic nanoparticles using red sanders powder extract as reducing agent. *Int. J. Polym. Anal. Charact.* 24 (4), 346–354. <https://doi.org/10.1080/1023666X.2019.1598631>.
- Rao, T.N., Riyazuddin, Babji, P., Ahmad, N., Khan, R.A., Hassan, I., Shahzad, S.A., Husain, F.M., 2019. Green synthesis and structural classification of *Acacia nilotica* mediated-silver doped titanium oxide (Ag/TiO₂) spherical nanoparticles: assessment of its antimicrobial and anticancer activity. *Saudi J. Biol. Sci.* 26 (7), 1385–1391.
- Rasineni, G.K., Siddavattam, D., Reddy, A.R., 2008. Free radical quenching activity and polyphenols in three species of *Coleus*. *J. Med. Plants Res.* 2, 285–291.
- Rather, R.A., Singh, S., Pal, B., 2017. Photocatalytic degradation of methylene blue by plasmonic metal-TiO₂ nanocatalysts under visible light irradiation. *J. Nanosci. Nanotechnol.* 17 (2), 1210–1216.
- Rostami-Vartooni, A., Nasrollahzadeh, M., Salavati-Niasari, M., Atarod, M., 2016. Photocatalytic degradation of azo dyes by titanium dioxide supported silver nanoparticles prepared by a green method using *Carpobrotus acinaciformis* extract. *J. Alloys Compd.* 689, 15–20.
- Saeed, M., Muneer, M., Khosa, M.K.K., Akram, N., Khalid, S., Adeel, M., Nisar, A., Sherazi, S., 2019. *Azadirachta indica* leaves extract assisted green synthesis of Ag-TiO₂ for degradation of methylene blue and rhodamine B dyes in aqueous medium. *Green Process Synth.* 8, 659–666.
- Saha, J., Begum, A., Mukherjee, A., Kumar, S., 2017. A novel green synthesis of silver nanoparticles and their catalytic action in reduction of Methylene Blue dye. *Sustain. Environ. Res.* 27 (5), 245–250.
- Santos, D.I., Neiva Correia, M.J., Mateus, M.M., Saraiva, J.A., Vicente, A.A., Moldão, M., 2019. Fourier transform Infrared (FT-IR) spectroscopy as a possible rapid tool to evaluate abiotic stress effects on pineapple by-products. *Appl. Sci.* 9 (19), 4141. <https://doi.org/10.3390/app9194141>.
- Sapkota, K., Chaudhary, P., Han, S.S., 2018. Environmentally sustainable route to SiO₂@Au–Ag nanocomposites for biomedical and catalytic applications. *RSC Adv.* 8 (55), 31311–31321.
- Sarina, S., Waclawik, E.R., Zhu, H., 2013. Photocatalysis on supported gold and silver nanoparticles under ultraviolet and visible light irradiation. *Green Chem.* 15 (7), 1814. <https://doi.org/10.1039/c3gc40450a>.
- Singh, J., Dhaliwal, A.S., 2020. Plasmon-induced photocatalytic degradation of methylene blue dye using biosynthesized silver nanoparticles as photocatalyst. *Environ. Technol.* 41 (12), 1520–1534.
- Sobana, N., Muruganadham, M., Swaminathan, M., 2006. Nano-Ag particles doped TiO₂ for efficient photodegradation of direct azo dyes. *J. Mol. Catal. A Chem.* 258, 124–132.
- Tahir, K., Ahmad, A., Li, B., Nazir, S., Khan, A.U., Nasir, T., Khan, Z.U.H., Naz, R., Raza, M., 2016. Visible light photo catalytic inactivation of bacteria and photo degradation of methylene blue with Ag/TiO₂ nanocomposite prepared by a novel method. *J. Photochem. Photobiol. B* 162, 189–198.
- Vanaja, M., Annadurai, G., 2013. *Coleus aromaticus* leaf extract mediated synthesis of silver nanoparticles and its bactericidal activity. *Appl. Nanosci.* 3, 217–223.
- Varma, R.S., Thorat, N., Fernandes, R., Kothari, D., Patel, N., Miotello, A., 2016. Dependence of photocatalysis on charge carrier separation in Ag-doped and decorated TiO₂ nanocomposites. *Catal. Sci. Technol.* 6, 8428–8440.
- Wahyuni, S., Syukri, Arief, S., 2019. Green synthesis of Ag/TiO₂ nanocomposite assisted by gambier leaf (*Uncaria gambir* Roxb) extract. *J. Kim. Sains Apl.* 22, 250–255.
- Xiang, Q., Yu, J., Cheng, B., Ong, H., 2010. Microwave-hydrothermal preparation and visible-light photoactivity of plasmonic photocatalyst Ag-TiO₂ nanocomposite hollow spheres. *Chem. Asian. J.* 5, 1466–1474.

- Yang, X., Fu, H., Wong, K., Jiang, X., Yu, A., 2013. Hybrid Ag@TiO₂ core-shell nanostructures with highly enhanced photocatalytic performance. *Nanotechnology* 24, 415601.
- Yu, J.G., Xiong, J.F., Cheng, B., Liu, S., 2005. Fabrication and characterization of Ag-TiO₂ multiphase nanocomposite thin films with enhanced photocatalytic activity. *Appl. Catal. B* 60, 211–221.
- Zahir, A.A., Chauhan, I.S., Bagavan, A., Kamaraj, C., Elango, G., Shankar, J., Arjaria, N., Roopan, S.M., Rahuman, A.A., Singh, N., 2015. Green synthesis of silver and titanium dioxide nanoparticles using *Euphorbia prostrata* extract shows shift from apoptosis to G₀/G₁ arrest followed by necrotic cell death in *Leishmania donovani*. *Antimicrob. Agents Chemother.* 59, 4782–4799.
- Zhang, H.J., Chen, G.H., 2009. Potent antibacterial activities of Ag/TiO₂ nanocomposite powders synthesized by a one-pot sol-gel method. *Environ. Sci. Technol.* 43, 2905–2910.